Article

J. Biol. Regul. Homeost. Agents. 2024; 38(9): 5845–5858
https://doi.org/10.23812/j.biol.regul.homeost.agents.20243809.466

METTL3 Promotes Intrahepatic Cholangiocarcinoma Progression by Enhancing S100A4 Expression in an m6A-Dependent Manner

Jie Sheng[1,2], Ying Zhu[1,2], Chenyue Zhang[1,2], Changjing Huang[1,2], Zhiqiang Meng[1,2,*]

[1]Minimally Invasive Treatment Center, Fudan University Shanghai Cancer Center, 200032 Shanghai, China
[2]Department of Oncology, Shanghai Medical College, Fudan University, 200032 Shanghai, China
*Correspondence: mengshca@fudan.edu.cn (Zhiqiang Meng)
Submitted: 7 May 2024 Revised: 1 June 2024 Accepted: 9 July 2024 Published: 30 August 2024

Background: Intrahepatic cholangiocarcinoma (ICC) is a prevalent type of cancer originating from epithelial cells of the bile duct within the liver. The molecular mechanisms underlying ICC proliferation, invasion, and metastasis remain unclear. Recently, N6-methyladenosine (m6A) RNA methylation has been associated with tumor progression. Methyltransferase 3 (METTL3) is a crucial methyltransferase for m6A. However, its biological significance and the regulatory mechanisms underlying ICC invasion and metastasis remain poorly understood. Therefore, we aimed to explore the role of METTL3 in ICC progression and its potential mechanisms.

Methods: We analyzed the expression of METTL3 in ICC using bioinformatics, quantitative reverse transcription polymerase chain reaction (qRT-PCR), and immunohistochemistry analysis. Furthermore, we evaluated the impact of METTL3 on ICC cell proliferation and metastasis *in vivo* and *in vitro*. For mechanistic studies, we used RNA-Seq to screen the crucial downstream targets of METTL3 in ICC cells. Furthermore, we examined the regulatory impact of METTL3 on the phenotype of ICC cells through S100 calcium-binding protein A4 (S100A4) using qRT-PCR, Western blot, and rescue experiments. Finally, we assessed the effect of METTL3 on S100A4 stability by mediating m6A modification using the methylated RNA immunoprecipitation qPCR (MeRIP-qPCR) and messenger RNA (mRNA) degradation experiments.

Results: The expression of METTL3 was upregulated in patients with ICC ($p < 0.05$). Moreover, METTL3 knockdown inhibited the proliferation, migration, and invasion ability of ICC cells ($p < 0.05$). Mechanistically, METTL3 mediated m6A modification of S100 calcium-binding protein A4 (*S100A4*) mRNA and inhibited *S100A4* mRNA decay in an m6A-dependent manner ($p < 0.05$), thus promoting the proliferation and metastasis of ICC.

Conclusions: METTL3 promotes ICC proliferation and metastasis by mediating *S100A4* mRNA degradation, suggesting that METTL3 may be a potential target for treating ICC.

Keywords: METTL3; m6A; S100A4; intrahepatic cholangiocarcinoma

Introduction

Intrahepatic cholangiocarcinoma (ICC) is a prevalent type of cancer arising from epithelial cells of the bile duct within the liver. It is the second most common primary liver cancer, accounting for approximately 15%–20% of all primary liver cancers [1]. The one-year overall survival rate for ICC patients is around 30%, while the 5-year overall survival rate is about 18% [2,3]. With the emergence of more effective chemotherapy and targeted medications, the combination of multidisciplinary treatment methods, including surgery, systemic therapy, and local radiation therapy, has extended the survival period for ICC patients to a certain extent [4,5]. However, the molecular mechanisms underlying ICC proliferation, invasion, and metastasis remain unclear. Therefore, it is crucial to unveil these mechanisms and identify novel molecular targets to enhance early disease diagnosis, development of new strategies, and improve prognostic assessment for ICC patients.

Epithelial-mesenchymal transition (EMT) is a significant mechanism for tumor progression and metastasis [6]. The hallmarks of EMT include the downregulation of epithelial molecules (e.g., E-cadherin) and the upregulation of mesenchymal cell molecules (e.g., N-cadherin, fibronectin, β-catenin, and S100 calcium-binding protein A4 (S100A4)) [7,8]. S100A4 has been reported to be significantly associated with vascular invasion, metastasis, and tumour, node and metastasis (TNM) staging in ICC [9].

As the "writer" in the N6-methyladenosine (m6A) system, methyltransferase 3 (METTL3) plays a critical catalytic role in regulating methylation transfer processes. METTL3 has been implicated in developing various tumors [10–12]. In ICC, upregulation of METTL3 leads to m6A modification of Interferon Induced Protein with Tetra-

Journal of
BIOLOGICAL REGULATORS
and Homeostatic Agents

tricopeptide Repeats 2 (*IFIT2*) messenger RNA (mRNA), promoting ICC progression and correlating with poorer prognosis [13]. Furthermore, METTL3 upregulates m6A of Nuclear Factor of Activated T Cells 5 (NFAT5), thereby recruiting Insulin Like Growth Factor 2 mRNA Binding Protein 1 (*IGF2BP1*) to stabilize *NFAT5* mRNA [14]. Activation of METTL3/Hepatic leukemia factor (HLF)/FOXQ1 regulatory circuit enhances Frizzled Class Receptor 4 (FZD4)-mediated Wingless and Int-1 (WNT)/β-catenin signaling in ICC progression [15]. However, the biological importance of METTL3 and the underlying mechanisms regulating ICC invasion and metastasis remain largely unknown. Additionally, the correlation between METTL3 and S100A4 in ICC has not been elucidated.

This study reveals a novel regulatory mechanism involving METTL3-mediated m6A modification in ICC. Our findings demonstrate that METTL3 regulates *S100A4* mRNA half-life in an m6A-dependent manner, suggesting the potential of METTL3 as a novel prognostic indicator and therapeutic target for ICC proliferation and metastasis.

Materials and Methods

Bioinformatics Analysis

We retrieved Gene Expression Omnibus (GEO) data (https://www.ncbi.nlm.nih.gov/geo/) and processed it using GEOquery, saving the eSet locally as raw data. The GSE107943 dataset was annotated using the annoprobe package (https://cran.r-project.org/web/packages/AnnoProbe/index.html). Box plots were generated using the GGpubr package (https://cran.r-project.org/web/packages/ggpubr/index.html), and statistical analysis was performed employing the Wilcoxon rank sum test. Furthermore, The Cancer Genome Atlas (TCGA) data was analyzed through http://gepia.cancer-pku.cn, and boxplot outputs were saved as PDF files.

RNA Extraction from Tissues

Total RNA was extracted from human ICC and adjacent non-cancer tissues previously embedded in OCT and stored at –80 °C. For this purpose, tissues were thawed at room temperature, washed with sterile Phosphate-Buffered Saline (PBS) and homogenized using the TRIzol reagent (Cat. No. 15596026, Thermo Fisher, Waltham, MA, USA). For ICC cell lines, cells from different experimental groups were collected and washed with PBS. Total RNA was extracted using TRIzol method following the manufacturer's instructions and quantified utilizing UV spectrophotometry (DS-11, DeNovix, USA). The extracted RNA was then stored at –80 °C for subsequent experimentations. The study was conducted following the Declaration of Helsinki and approved by the Ethics Committee of Fudan University Shanghai Cancer Center, China (FUSCC-IACUC-S2022-0622). Furthermore, all the study participants provided written informed consent.

Quantitative Reverse Transcription Polymerase Chain Reaction (qRT-PCR)

The total RNA was reverse transcribed into cDNA using PrimeScript™ RT Master Mix (#RR036A, Takara, Shiga, Japan). Quantitative PCR was performed employing a LightCycler 480II real-time PCR system (Roche, Basel, Switzerland). At the completion of the reaction, the cycle threshold (CT) was determined, and the relative expression levels of the target genes were assessed using the $2^{-\Delta\Delta Ct}$ method. The primer sequences used in qPCR were as follows: glyceraldehyde-3-phosphate dehydrogenase (*GAPDH*)-5′-AAGGTGAAGGTCGGAGTCAAC-3′ and 5′-GGGGTCATTGATGGCAACAATA-3′; *METTL3*-5′-CGTACTACAGGATGATGGCTTTC-3′ and 5′-TTTCATCTACCCGTTCATACCC-3′; *S100A4*-5′-TCAGAACTAAAGGAGCTGCTGACC-3′ and 5′-TTTCTTCCTGGGCTGCTTATCTGG-3′.

Western Blot

Cells from different experimental groups were collected and lysed in Mammalian Protein Extraction Reagent (M-PER, 78505, Thermo Fisher, Waltham, MA, USA) supplemented with a protease inhibitor cocktail. Proteins were resolved through SDS-PAGE and transferred onto polyvinylidene difluoride (PVDF) membranes. The membranes were blocked with 5% skim milk in TBST for 1 hour at room temperature, followed by sequential incubation with primary antibodies (dilution ratio, 1:1000) and secondary antibodies (dilution ratio, 1:5000). After this, they were incubated with HRP substrate luminol reagent (WBKLS0500, Millipore, Bedford, MA, USA) and exposed to ChampChemi professional plus (SG2010084, SageCreation, Beijing, China). The primary antibodies used in Western blot analysis were as follows: anti-METTL3/MT-A70 (Bethyl, Montgomery, TX, USA, Cat. No. A301-568A, RRID: AB_1040003; Proteintech, Wuhan, China, Cat. No. 15073-1-AP, RRID: AB_2142033), anti-β-actin (Cat. No. MA5-15739, Thermo Fisher, Waltham, MA, USA), and anti-S100A4 (ab58597, Abcam, Cambridge, UK). Moreover, secondary antibodies included Donkey anti-rabbit IgG-HRP (Cat. No. sc-2077, Santa Cruz Biotechnology, Dallas, TX, USA) and Goat anti-mouse IgG-HRP (Cat. No. sc-2055, Santa Cruz Biotechnology, Dallas, TX, USA). Finally, membranes were observed and protein images were quantified using Image J 1.53a software (National Institutes of Health, Bethesda, MD, USA).

mRNA Enrichment and m6A Dot-Blot Analysis

Total RNA underwent mRNA enrichment using a Dynabeads mRNA Purification Kit (61006, Invitrogen, Waltham, MA, USA), and m6A levels were assessed employing Dot-Blot analysis. After this, the resultant RNA was diluted, heated to denature secondary structures, and transferred onto Hybond-N+ nylon membranes (RPN303B,

GE Healthcare, Chicago, IL, USA) for UV crosslinking. The membranes were then blocked, stained with methylene blue for total RNA visualization, and probed with an anti-m6A antibody (1:500, Synaptic Systems, Goettingen, Germany, Cat. No. 202003, RRID: AB_2279214). Finally, images were captured using a Tanon4500 system (Shanghai, China) under white light and fluorescence settings. Subsequently, m6A and methylene blue staining levels were quantified with Image J 1.53a software (National Institutes of Health, Bethesda, MD, USA).

m6A Enzyme-Linked Immunosorbent Assay (ELISA)

The m6A RNA Methylation Quantification Kit (ab185912, Abcam, Cambridge, UK) was used to determine m6A levels in RNA. For this purpose, each well was added with 80 µL of Binding Solution and then covered, followed by incubation at 37 °C for 90 minutes. After removing the binding solution, 150 µL of 1× wash buffer was added to each well and washed 3 times. In the next step, 50 µL of Capture Antibody was added to each well and incubated at room temperature for 60 minutes. After washing each well, 50 µL of dilute enhancer solution was added and incubated at room temperature for 30 minutes. Subsequently, each well was washed five times with 150 µL of 1× wash buffer. Upon observing color changes in the positive control wells, 100 µL of stop solution was added to each well, and the absorbance at 450 nm was assessed using a microplate reader within 2 to 10 minutes. The percentage of m6A in RNA was calculated using the following formula:

Cell Culture

Human intrahepatic cholangiocarcinoma cell lines, RBE and HCCC-9810, were obtained from the National Biomedical Experimental Cell Resource Bank (1101HUM-PUMC000675 and 1101HUM-PUMC000278). However, ICC 4389 cells were human intrahepatic cholangiocarcinoma cells and were kindly given by 3D Biomedicine Science and Technology Co., Ltd. (Shanghai, China). RBE and HCCC-9810 cells were cultured in RPMI-1640 complete medium supplemented with 10% fetal bovine serum (5669701, Gibco, Waltham, MA, USA) and 1% penicillin/streptomycin. However, 4389 cells were cultured in DMEM complete medium supplemented with 10% FBS and 1% penicillin/streptomycin. These cell cultures were maintained in a constant temperature incubator at 37 °C with 5% CO_2. The culture medium was refreshed the next day after cell recovery. Upon reaching 80%–90% confluence, the cells were passaged using PBS, and trypsin was utilized to detach the cells. After this, cells were collected, centrifuged, and resuspended in a fresh, complete medium for subsequent experiments. Cells were passaged at a ratio of 1:5 and used for experiments after 2–3 passages. Cells in the exponential growth phase were selected for cryopreservation. These cell lines were authenticated using short tandem repeat (STR) profiling and examined for contamination employing mycoplasma assay.

Cell Proliferation Assay

The cells were enzymatically digested and resuspended to a concentration of 2×10^4 cells/mL. Subsequently, 0.1 mL of cell solution was added to each well of a 96-well plate, with 3 replicates per experimental group. Cell proliferation was monitored at fixed time points for 5 consecutive days (0 hours, 24 hours, 48 hours, 72 hours, and 96 hours). At each time point, 10 µL of cell counting kit 8 (CCK8) reagent was added to each well and incubated at 37 °C for 2 hours. Finally, the optical density (OD) value was measured at 450 nm utilizing a microplate reader, and the growth curve was generated based on these observations.

Virus Transfection

All the knockdown lentiviruses in this study were packaged by GeneChem, Co. (Shanghai, China), using GV493-EGFP-Puro vectors. Lentivirus particles were packaged with the pHelper 1.0 packaging vector (GeneChem, Co., Shanghai, China). and the pHelper 2.0 packaging vector (GeneChem, Co., Shanghai, China). using the Lenti-easy packaging system (GeneChem, Co., Shanghai, China). The specific sequences used for sh*METTL3* were as follows: sh*M3*-1: gcGGAGATCCTAGAGCTATTA and sh*M3*-2: gcTGCACTTCAGACGAATTAT. The S100A4 (Gene ID: 6275, NM_002961.3) overexpression virus was also packaged by GeneChem, Co. using GV492-gcGFP-Puro vectors (GeneChem, Co., Shanghai, China).

For transfection, the virus was thawed on ice, and an appropriate volume was added to Opti-MEM medium (31985088, Gibco, Waltham, MA, USA, 500 µL/well), along with Hitrans-A (20×) transfection reagent. The cell culture medium was replaced with 500 µL Opti-MEM, and the virus dilution was added to each well. Once satisfactory transfection efficiency was confirmed, subsequent experiments were then performed.

Transwell Assay

Pre-chilled Matrigel was diluted tenfold using Opti-MEM (Gibco, 31985070, Waltham, MA, USA). Then, 100 µL of the diluted Matrigel was added to the upper chamber of the Transwell insert and incubated at a constant temperature for 2 hours in a cell culture incubator. After this, the supernatant was removed, and subsequent experiments were performed. Following cell digestion in each group, 700 µL of the appropriate complete medium containing serum was added to the lower chamber of Transwell. The cells were seeded at a density of 4–10 $\times$ 10^5 cells in each Transwell chamber, with or without Matrigel, and incubated for 24 hours. After incubation, cells were harvested, immersed in pre-chilled PBS, and washed three times. The cells were

Journal of
BIOLOGICAL REGULATORS
and Homeostatic Agents

fixed with 4% paraformaldehyde for 15 minutes. The upper layer of cells was gently wiped off with a wet cotton swab and stained with crystal violet dye. Cells were observed using a microscope, and images were captured with a 10× objective lens. Finally, cells were counted using Image J software for quantitative analysis.

RNA-Seq

Total RNA from RBE and 9810 cells was isolated using TRIzol reagent (15596018, Thermo Fisher, Waltham, MA, USA). The integrity of RNA was examined by checking RIN numbers using an Agilent Bioanalyzer 2100 (Agilent Technologies, Santa Clara, CA, USA). Qualified total RNA was purified using the RNAClean XP Kit (A66514, Beckman Coulter, Brea, CA, USA) and treated with RNase-Free DNase (79254, QIAGEN, Dusseldorf, Germany).

For RNA-Seq, libraries were created using the VAHTS Universal V6 RNA-Seq Library Preparation Kit for Illumina® (NRM605-02, Vazyme, Nanjing, China). Sequencing was conducted on an Illumina HiSeq 2000S platform, generating single-end reads with a length of 200–300 bp. The sequence reads were compared to the GRCH38 reference genome using standard Illumina sequence analysis pipelines. The subsequent analysis was based on average gene expression values obtained from two independent experiments.

Experimental Animals

For the subcutaneous tumor experiments, male nude mice (n = 30), aged 5–6 weeks and weighing about 18 grams, were procured from Shanghai Jihui Experimental Animal Breeding Co., Ltd. (Shanghai, China). They were housed in a specific pathogen-free (SPF) animal facility within the animal center. The animal experiments were conducted following legal requirements, including federal, state, and local laws and regulations. All animals were lawfully acquired and their retention and use were in every case in compliance with federal, state and local laws and regulations, and in accordance with the Institutional Animal Care and Use Committee of SHCO (IACUC) Guide for Care and Use of Laboratory Animals (SHCO-20200042).

One day before the tumor experiment, 2 mL of Matrigel was thawed in a refrigerator at 4 °C and experimental consumables were pre-chilled, such as pipette tips, at –20 °C. The logarithmic growth phase 4389 cells from each experimental group (shNC, shM3-1, and shM3-2) were digested as previously described. They were counted and centrifuged at a density of 10×10^7 cells/mL. After disinfecting the skin around the injection site on the right side of the axilla of nude mice with 75% medical alcohol, 100 µL of cell suspension was subcutaneously administered. Tumor growth was monitored every 3 days.

Upon reaching tumor diameter at 1.0–1.5 cm in the control group, mice were euthanized through intraperitoneal injection of pentobarbital (250 mg/kg). The tumors were harvested, photographed, weighed, and preserved in formalin solution or a –80 °C for subsequent experiments.

HE Staining and Immunohistochemistry

After isolation, tumors were fixed in 4% formaldehyde, paraffin-embedded and sectioned into slices. Hematoxylin and eosin (HE) staining (ab245880, Abcam, Cambridge, UK) was performed following standard protocols. For immunohistochemistry, tumor tissue sections underwent heat-induced epitope retrieval using the histochemistry kit (SP 900, ZSGB-BIO, Beijing, China). After this, tissue sections were incubated overnight with Ki-67 antibody (Abcam, Cambridge, UK, ab15580, dilution ratio, 1:50) at 4 °C. The next day, they were incubated with 100 uL HRP-conjugated secondary antibodies preconfigured in the ZSGB-BIO Kit (PV-9000, ZSGB-BIO, Beijing, China), followed by DAB staining (ZLI-9018, ZSGB-BIO, Beijing, China). Finally, slides were examined and photographed using an optical microscope (LV150N, Nikon, Tokyo, Japan). The immunohistochemistry (IHC) scoring was conducted according to the Allred scoring system [16–18]. The percentage of METTL3-positive cancer cell nuclei was categorized as follows: 1 for less than 1%, 2 for 1 to 10%, 3 for 11 to 33%, 4 for 34 to 66%, and 5 for more than 67%. The staining intensity of cell nuclei was scored as 1 for weak, 2 for medium, and 3 for strong. However, the total score ranged from 0 to 8, which was achieved by combining these scores. The Allred score provides a quantitative method to assess staining outcomes, assisting clinical decisions and research analysis.

Methylated RNA Immunoprecipitation qPCR (MeRIP-qPCR)

The MeRIP kit (Bes5203-1, Bersin Bio, Guangzhou, China) was used to examine m6A modifications on specific genes. Approximately 200 mg of RNA was isolated from RBE, and 4389 cells were fragmented to ~300 nucleotides and subsequently purified using IP buffer (450 µL) containing RNase inhibitor. A portion (1/9) of the fragmented product was applied as input. The m6A antibody was incubated with Protein A/G magnetic beads for 1 hour at 4 °C. After this, the beads were washed with IP buffer, and the m6A IP fraction was eluted and purified. The qTR-PCR analysis was conducted on the MeRIP-ed RNA samples.

RNA Stability

Cells from the shNC and shM3-1 groups were seeded in 6-well plates. After 24 hours, cells from each experimental group were treated with actinomycin D (Cat. No. A9415, Sigma-Aldrich, Burlington, MA, USA) at a final concentration of 5 mg/mL. After this, the cells were harvested at indicated time points (0, 24, 36 or 48 hours) and washed with PBS. Subsequently, RNA was extracted from these cells. Finally, to assess RNA stability, RT-qPCR

analysis was performed to determine residual RNA levels, which were normalized to the shNC group at a 0-hour time point.

Statistical Methods

Statistical analysis was performed using Prism GraphPad 9 (Version 9.5.0, Dotmatics, Boston, MA, USA). Each experiment was repeated three times to ensure statistical significance. Quantitative data were expressed as mean ± standard. For the data exhibiting normal distribution, the comparisons between two independent samples were performed using Student's *t* test. For proliferation analysis, differences among multiple groups were determined using one-way analysis of variance (ANOVA), followed by post hoc Bonferroni tests for multiple comparisons. Statistical analysis of public databases was performed using the Wilcoxon rank sum test. A p-value < 0.05 was considered statistically significant.

Results

Abnormal Increase of m6A Modification in ICC

We analyzed the data from publicly available databases to explore the role of METTL3 and m6A modifications in ICC. Analysis of the TCGA database revealed that METTL3 expression was significantly higher in ICC ($p < 0.05$) compared to adjacent non-cancer tissues (Fig. 1A). Subsequently, we retrieved a transcriptome sequencing dataset (GSE107943), which showed increased METTL3 expression in ICC tissues ($p < 0.05$) compared to adjacent non-cancer tissues (Fig. 1B). To further confirm these observations, we randomly selected 7 pairs of previously collected ICC and adjacent non-cancer tissue samples from our research group (Fig. 1C). The experimental findings from our samples were consistent with the outcomes obtained in the public databases, validating the elevated expression of METTL3 in ICC tissues ($p < 0.05$).

Additionally, we conducted METTL3 protein immunohistochemistry staining on 25 ICC cases and their adjacent tissues (Fig. 1D). The ICC scoring was performed by a skilled pathologist at our center and the findings are presented in Fig. 1E. It was observed that the expression level of METTL3 protein was significantly higher in intrahepatic cholangiocarcinoma tissues compared to paracancerous tissues ($p < 0.05$).

Given that m6A methylation modification is a dynamic process and METTL3 is a key methyltransferase component of the m6A system, mRNA was extracted from randomly selected pairs of ICC and adjacent non-cancer tissues to assess m6A modification levels using m6A Dot-Blot (Fig. 1F) and m6A ELISA kit (Fig. 1G). The findings indicated substantially elevated m6A levels in cancer tissues compared to adjacent non-cancer tissues ($p < 0.05$).

Knockdown of METTL3 in ICC Cells Inhibits Proliferation and Metastasis in Vitro

We established stable METTL3 knockdown cell lines specific to intrahepatic cholangiocarcinoma. Initially, we examined the impact of shNC on METTL3 expression compared to controls using qRT-PCR in different ICC cell lines and observed no difference between the two groups (**Supplementary Fig. 1**). Therefore, we used shNC as a control instead of control wild-type ICC cells in subsequent experiments.

Subsequently, HCCC-9810, RBE, and 4389 cells were transfected with lentiviral vectors containing two different shRNA fragments to construct METTL3 stable knockdown ICC cell lines. The changes in *METTL3* mRNA expression after transfection were evaluated using qRT-PCR. As depicted in Fig. 2A, *METTL3* mRNA expression levels were significantly alleviated in the METTL3 knockdown groups of RBE, HCCC-9810, and 4389 cell lines compared to the NC group ($p < 0.05$), confirming successful METTL3 knockdown. After this, total RNA was extracted from each group of cells and enriched, followed by relative quantification of mRNA m6A levels and m6A Dot-Blot experiments using an m6A methylation ELISA kit. As shown in Fig. 2B, the m6A level in ICC cells decreased significantly following METTL3 knockdown. Moreover, the findings from the m6A methylation ELISA kit confirmed a significant decrease in mRNA m6A modification levels in ICC cells after METTL3 knockdown (Fig. 2C).

Furthermore, the CCK8 assay was used to assess the differences in the proliferation ability of ICC cells between control and knockdown groups. We found that the absorbance at 450 nm was significantly reduced ($p < 0.05$) in RBE, HCCC-9810, and 4389 cells at 96 hours after METTL3 knockdown compared to control cells (Fig. 2D). Furthermore, we examined the effect of interfering with METTL3 expression on the proliferative ability of RBE, HCCC-9810, and 4389 cells using clone formation assays. As shown in Fig. 2E, after 14 days of incubation, the cells in METTL3 knockdown group formed fewer clones than the corresponding control group, indicating that knockdown of METTL3 expression significantly inhibited the proliferation of various ICC cells ($p < 0.05$).

The Transwell assay was used to test the invasive and migratory abilities of ICC cells after *METTL3* knockdown. Transwell assay chambers with or without matrix gel were used to examine the invasive and migratory abilities of the cells, respectively. Due to the clustered growth characteristics of 4389 cells, the percentage of the area covered by 4389 cells was used to evaluate invasive and migratory abilities instead of counting cells that penetrated the polycarbonate membrane. Additionally, the Transwell assay demonstrated that the cell migration and invasion capabilities were substantially reduced in the *METTL3* knockdown

Journal of
BIOLOGICAL REGULATORS
and Homeostatic Agents

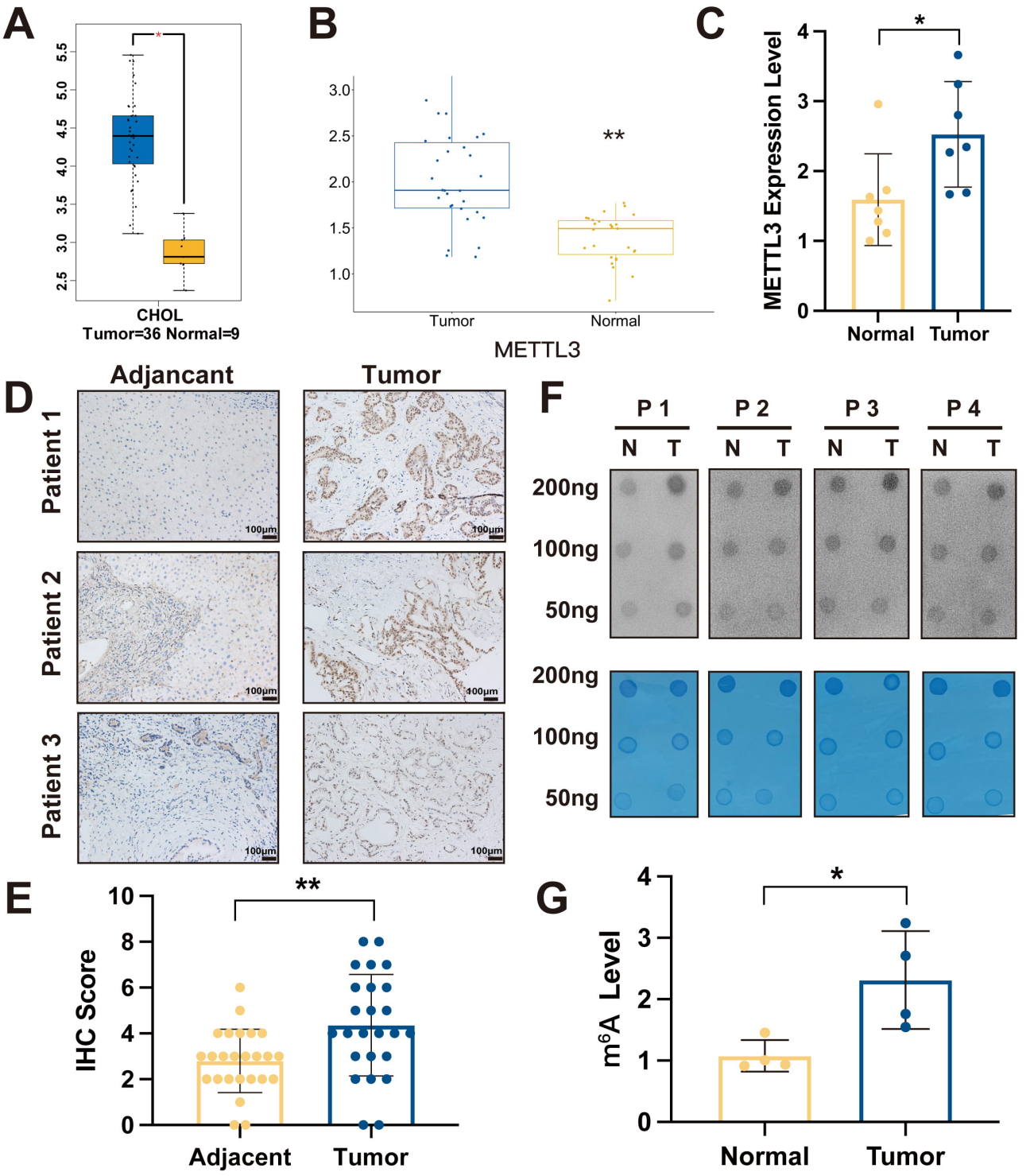

Fig. 1. The expression levels of METTL3 in ICC. (A) Differences of METTL3 in cholangiocarcinoma tumor tissues (Blue, n = 36) and adjacent non-cancer tissues (Yellow, n = 9) in the TCGA database (GEPIA, http://gepia.cancer-pku.cn/detail.php?gene=). (B) GSE107943 dataset included RNA-Seq data from ICC patients (n = 30) and paired adjacent non-cancer tissues (n = 26) from Keimyung University Dongsan Medical Center in Korea. (C) *METTL3* mRNA levels in cancer and adjacent tissues from ICC patients (n = 7). (D) Immunohistochemistry staining results of METTL3 in 3 cases of ICC tissues or adjacent non-cancer tissues (n = 3). (E) Statistical chart of METTL3 scoring in 25 ICC cases or adjacent non-cancer tissues (n = 25). (F,G) Difference in mRNA N6-methyladenosine (m6A) modification levels between ICC tissues and adjacent non-cancer tissues (n = 4). *$p < 0.05$; **$p < 0.01$. ICC, intrahepatic cholangiocarcinoma; METTL3, methyltransferase 3; TCGA, The Cancer Genome Atlas; GEPIA, Gene Expression Profiling Interactive Analysis; mRNA, messenger RNA; IHC, immunohistochemistry.

group compared to the control group (Fig. 2F,G, $p < 0.05$). These results imply that targeting METTL3 could be an effective therapeutic approach for treating ICC.

METTL3 Promotes ICC Progression in Vivo

Nude mice were administered with 1×10^7 cells from each group of 4389 cells (shNC, shM3-1, and shM3-2), and all developed tumors. Tumor size was considerably smaller in the METTL3 knockdown group ($p < 0.05$) compared to mice in the NC group (Fig. 3A). After this, tumor tissues were isolated and subjected to HE staining and Ki-67 immunohistochemistry. The HE staining demonstrated tubular structures within the tumors, indicating that the subcutaneous tumors in mice originated from the proliferation of the cholangiocarcinoma cells that we inoculated. Additionally, as shown in Fig. 3B, the Ki-67 staining intensity was weaker in the tubular-like structures of tumors from the METTL3 knockdown group, suggesting the increased proliferative capacity of ICC cells *in vivo*. These findings demonstrate the critical role of METTL3 in enhancing ICC progression *in vivo*.

METTL3 Mediates the Expression of S100A4

We performed high-throughput mRNA sequencing to investigate the mechanism by which METTL3 regulates ICC cell proliferation and invasion and to identify downstream molecules. The phenotypes of RBE, 9810, and 4389 were examined in this study *in vitro*, suggesting that METTL3 exerts the same effect on these three cell lines. Therefore, we focused on hcc-9810 and RBE cells to assess changes in downstream gene expression before and after METTL3 interference. As shown in Fig. 4A, a strong correlation was observed among the six cell groups, indicating uniform differential gene expression profiles between control and METTL3-interfered ICC cells. We identified intersecting downregulated genes in RBE shNC, RBE shM3-1 and shM3-2, and HCCC-9810 shNC, HCCC9810 shM3-1, and shM3-2 (Fig. 4B). Subsequently, the intersection of these four groups demonstrated differential expression of genes ($|\log2FC| \geq 0.58$, $p < 0.01$). The downregulated genes included *EFNB2, S100A4, HS3ST1*, and *MMP7*, while upregulated genes included *MSMO1*, *NXN*, *RAB3D*, *RPUSD4*, *GABARAPL1*, *INSIG1*, *IER3IP1*, and *MMP24* (Fig. 4C). Importantly, *S100A4* was strongly associated with tumor metastasis in ICC.

Furthermore, to validate the regulatory effects of METTL3 on *S100A4*, we performed RT-PCR and Western blot analyses on RBE, HCCC-9810, and 4389 cells after METTL3 knockdown, along with their corresponding negative control cells. Compared to the control group, the expression of S100A4 in ICC cells HCCC-9810, RBE, and 4389 was decreased ($p < 0.05$) at the mRNA levels (Fig. 4D) and protein levels (Fig. 4E,F) after interfering with METTL3. These results indicate that METTL3 positively regulates S100A4 expression in ICC cells.

METTL3 Facilitates ICC Progression and Metastasis by Upregulating S100A4

To verify whether the inhibition of proliferation and invasion of intrahepatic cholangiocarcinoma cells caused by interfering with METTL3 expression is mediated by S100A4, we overexpressed S100A4 in METTL3-interfered (shM3-1) ICC cells and determined the expression levels of S100A4 (Fig. 5A–C). As the phenotypes of RBE, 9810 and 4389 were examined after METTL3 knockdown *in vitro*, suggesting that METTL3 has the same effect on these three cell lines. Therefore, we selected RBE and 4389 cells as study objects to study in this part. The impact of transfecting *S100A4* overexpression plasmid on the proliferation ability of RBE and 4389 cells was assessed using CCK8 assay. As expected, overexpression of S100A4 rescued the proliferation (Fig. 5D) of METTL3 knockdown ICC cells ($p < 0.05$).

Furthermore, we used Transwell assays to assess changes in the invasion and migration abilities of METTL3-interfered ICC cells after overexpressing *S100A4*. Due to the clustered proliferation characteristics of 4389 cells, individual cell counting was difficult. Therefore, we assessed invasion and migration capacity by measuring the percentage of area covered by 4389 cells rather than counting the number of cells that crossed the polycarbonate membrane. The experimental results from both 4389 and RBE cells confirmed that overexpression of *S100A4* partially or fully restored the inhibition of invasion and migration abilities in 4389sh and RBEsh cells (Fig. 5E–G). Our experimental data suggest that METTL3 promotes ICC progression by upregulating S100A4 expression.

METTL3 Prolongs S100A4 mRNA Stability by Regulating m6A Methylation

We used the RMbase database to predict the mRNA m6A sites of S100A4 and identified m6A methylation modification sites of S100A4 based on the sequencing results from dataset GSE37005. The m6A modification sequence of this gene is shown in Fig. 6A. Subsequently, we performed m6A enrichment using RNA from cells in distinct groups, followed by qPCR using primers designed for the highly methylated region of *S100A4* mRNA. The m6A levels of mRNA were then quantified for the control and METTL3 interference groups (as a percentage relative to input). As illustrated in Fig. 6B, the m6A methylation level of *S100A4* mRNA substantially decreased after interfering with METTL3. These findings demonstrate that interfering with METTL3 leads to decreased expression of S100A4 and reduced m6A modification levels of *S100A4* mRNA ($p < 0.05$).

Furthermore, we explored whether the half-life of *S100A4* mRNA in 4389 cells changed after interfering with METTL3. We used actinomycin D to measure the mRNA half-life of S100A4 in control and METTL3-interfered 4389 cells. As the above experimental results revealed con-

Journal of
BIOLOGICAL REGULATORS
and Homeostatic Agents

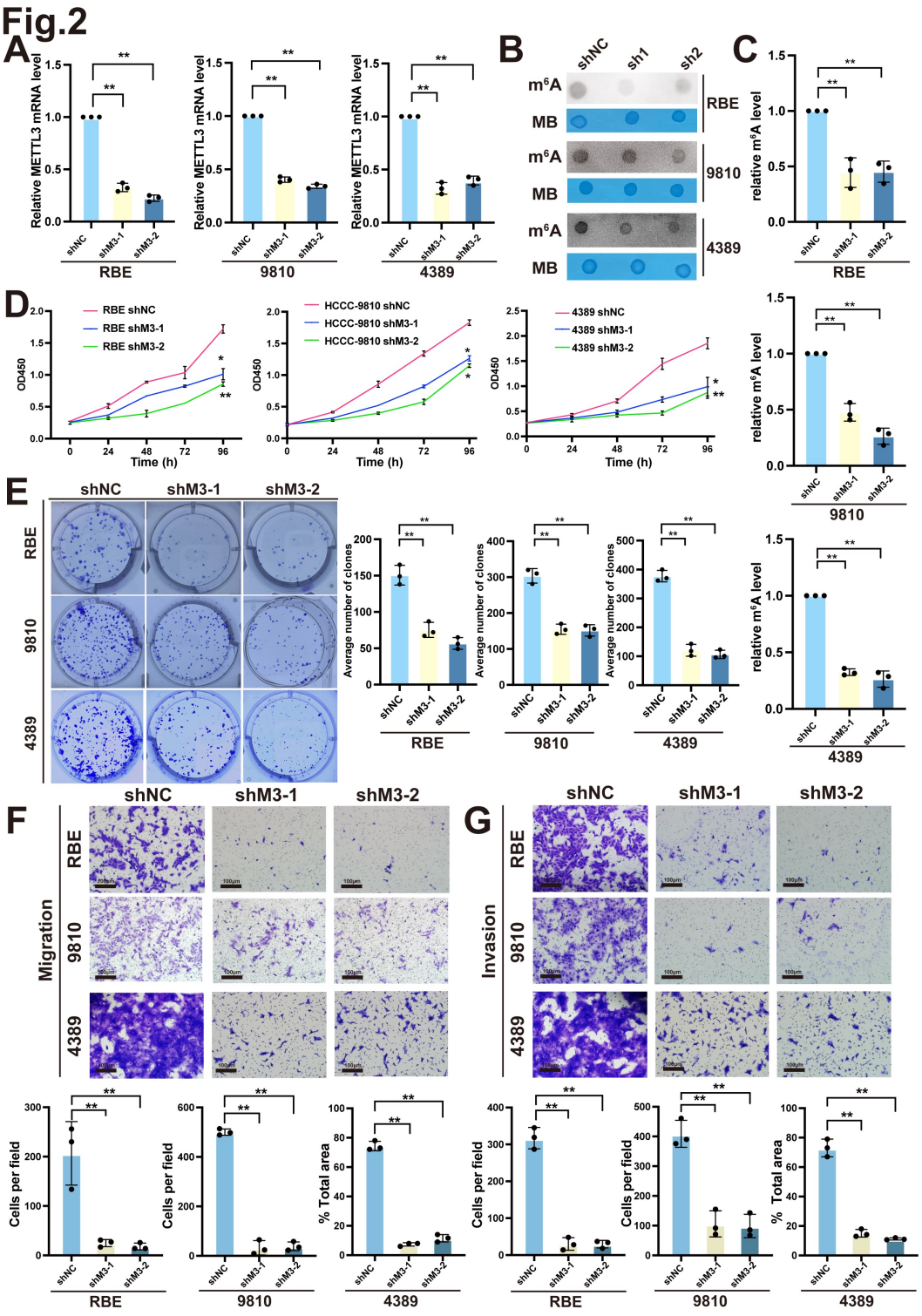

Fig. 2. METTL3 knockdown inhibits ICC proliferation and metastasis *in vitro*. (A) qRT-PCR analysis of *METTL3* mRNA in ICC cells (n = 3). (B) m6A Dot-Blot assays. MB, methylene blue staining. (C) The m6A methylation ELISA kit assesses changes in mRNA m6A (n = 3). (D) Cell counting kit 8 (CCK8) assays were used to assess changes in the proliferation following METTL3 knockdown in ICC cells (n = 3). (E) The colony formation experiment showed the difference in the cell clones between the METTL3 knockdown group and the shNC group after 14 days of long-term proliferation (n = 3). (F) Cell migration abilities of RBE, HCCC-9810, and 4389 cells after knocking down METTL3 (n = 3). (G) Cell invasion abilities of RBE, HCCC-9810, and 4389 cells after METTL3 knockdown (n = 3). $*p < 0.05$; $**p < 0.01$. qRT-PCR, quantitative reverse transcription polymerase chain reaction; ELISA, enzyme-linked immunosorbent assay.

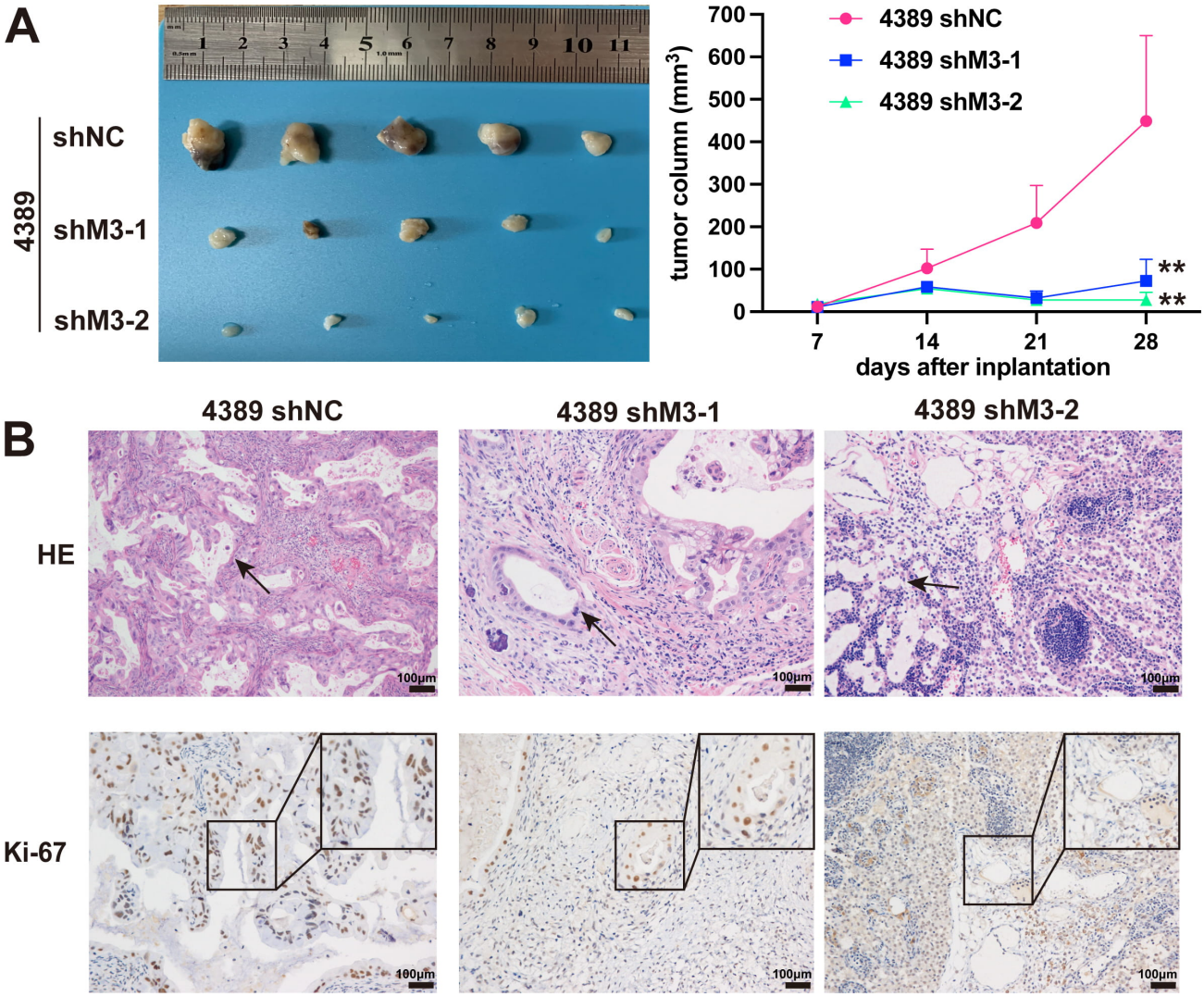

Fig. 3. Knockdown of METTL3 suppresses ICC progression *in vivo*. (A) Tumor volume in mice inoculated with 4389 cells (shNC, shM3-1 and shM3-2) (n = 5). $^{**}p < 0.01$. (B) Tumor tissues were subjected to HE staining and Ki-67 immunohistochemistry. The arrow indicates the tubular structure. HE, hematoxylin and eosin.

sistent effects of interference fragments, we selected shM3-1 for the mechanism verification experiments. RNA was extracted from cells treated with actinomycin D for 0 h, 24 h, 36 h, and 48 h, followed by qRT-PCR to evaluate changes in *S100A4* mRNA expression. The results demonstrated a significant alleviation in the half-life of *S100A4* mRNA in RBE cells ($p < 0.05$) after interfering with METTL3 (Fig. 6C), indicating that METTL3 can inhibit the degradation of *S100A4* mRNA and prolong its half-life in ICC cells.

Discussion

Numerous studies have investigated the role of METTL3 in various tumors, indicating conflicting results. While many investigations indicate that METTL3 acts as an oncogene in tumors [19–23], some studies have reported its anti-cancer effects [24–30]. In this study, we initially used bioinformatics methods to investigate the differential expression of METTL3 in ICC tissues compared to adjacent normal tissues. Subsequently, we validated these findings using ICC and adjacent tissues obtained from our center, confirming increased expression in ICC tissues. Additionally, we randomly selected 4 cases of ICC tissues and adjacent normal tissues for m6A Dot-Blot analysis to examine the m6A methylation modification levels in tumor tissues compared to adjacent tissues. The results revealed substantially elevated levels of m6A methylation modification level in ICC tissues compared to corresponding adjacent tissues.

Furthermore, we explored the effects of METTL3 on the proliferation, migration, and invasive capabilities of ICC cells *in vitro* and *in vivo*. These findings demonstrated that METTL3 could be a prospective target for treating ICC, especially metastatic tumors. Our findings align with Xu

Journal of
BIOLOGICAL REGULATORS
and Homeostatic Agents

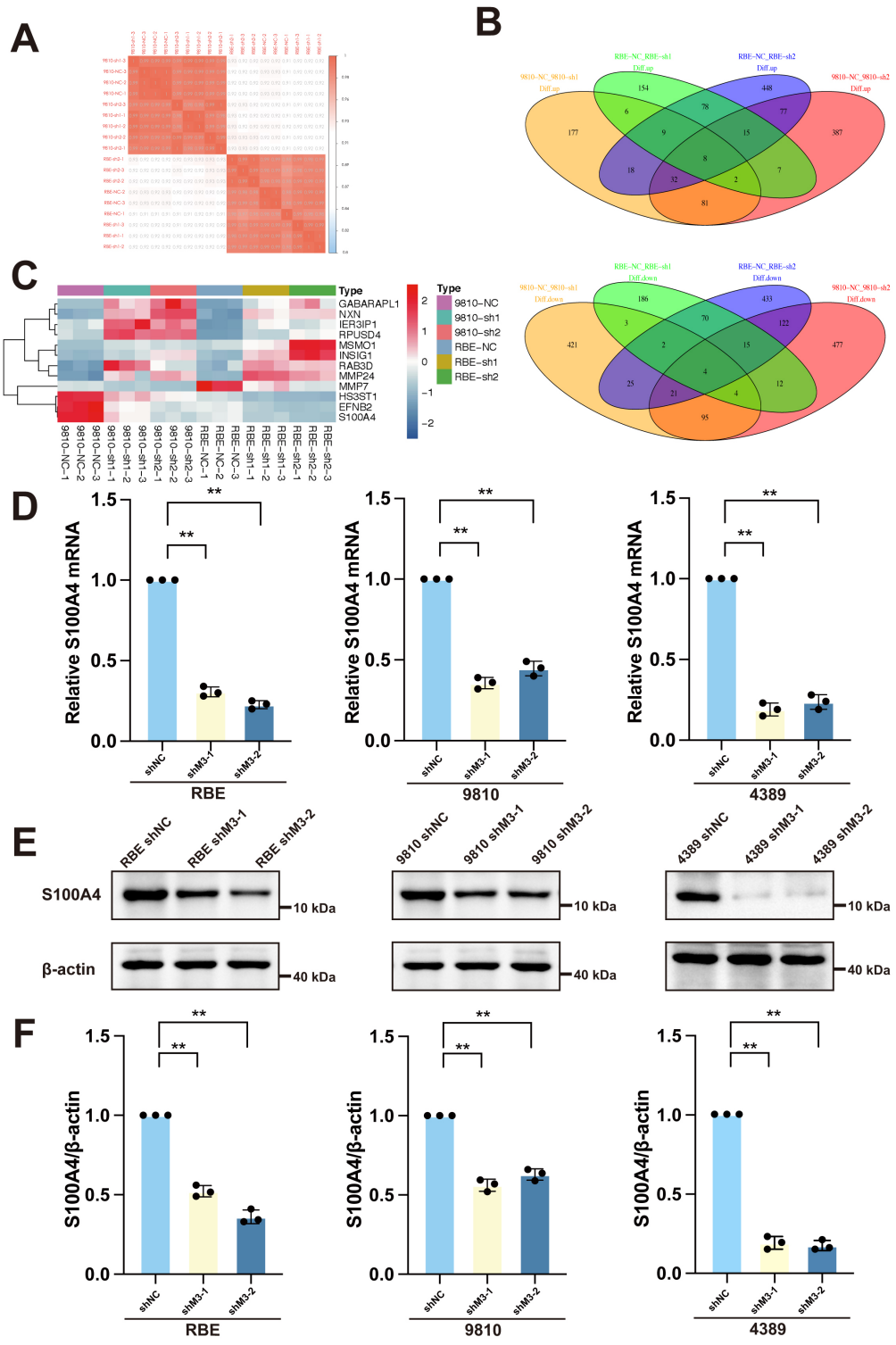

Fig. 4. S100A4 is a target downstream of *METTL3*. (A) Correlation among the six cell groups [(RBE shNC, RBE shM3-1 and shM3-2), and (HCCC-9810 shNC, HCCC9810 shM3-1, and shM3-2)]. (B) Differential gene expression profiles between control and METTL3-interfered ICC cells, followed by the intersection of the four groups of the differentially expressed genes ($|\log2FC| \geq 0.58$, $p < 0.01$). (C) Genes were differentially expressed in ICC cells after interfering with METTL3 expression. Upper panel: upregulated genes shared between RBE and 9810 cells. Lower panel: downregulated genes shared between RBE and 9810 cells. (D) Changes in S100A4 expression were determined using qRT-PCR analysis (n = 3). (E,F) Western blot analysis (E) and corresponding statistical results (F) of S100A4 in RBE, HCCC-9810, and 4389 cells interfered with METTL3 and their corresponding negative control cells (n = 3). $^{**}p < 0.01$. S100A4, S100 calcium-binding protein A4.

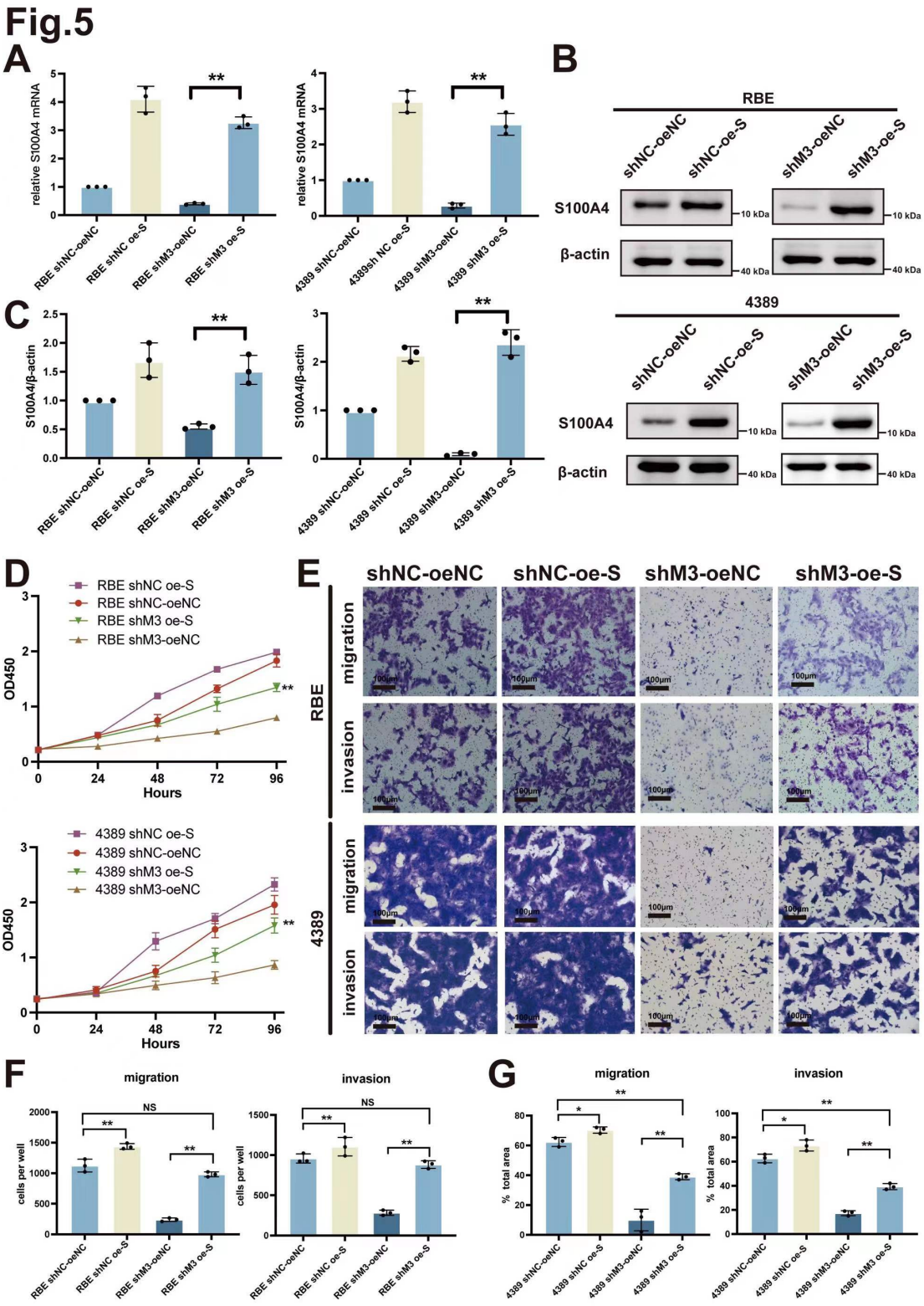

Fig. 5. ***METTL3*** **promotes the ICC by upregulating S100A4.** (A–C) qRT-PCR (A) and Western blot (B,C) analysis of S100A4 expression in distinct groups of ICC cells (n = 3). (D) CCK8 assays showed changes in the proliferation after *S100A4* overexpression in METTL3 knockdown ICC cells (n = 3). (E) Changes in the migration and invasion capabilities after overexpressing *S100A4* in *METTL3* knockdown ICC cells. (F,G) Statistical analysis of the migration and invasion abilities after overexpressing *S100A4* in RBE cells (F) and 4389 cells (G) (n = 3). *$p < 0.05$; **$p < 0.01$; NS, no significance.

Journal of
BIOLOGICAL REGULATORS
and Homeostatic Agents

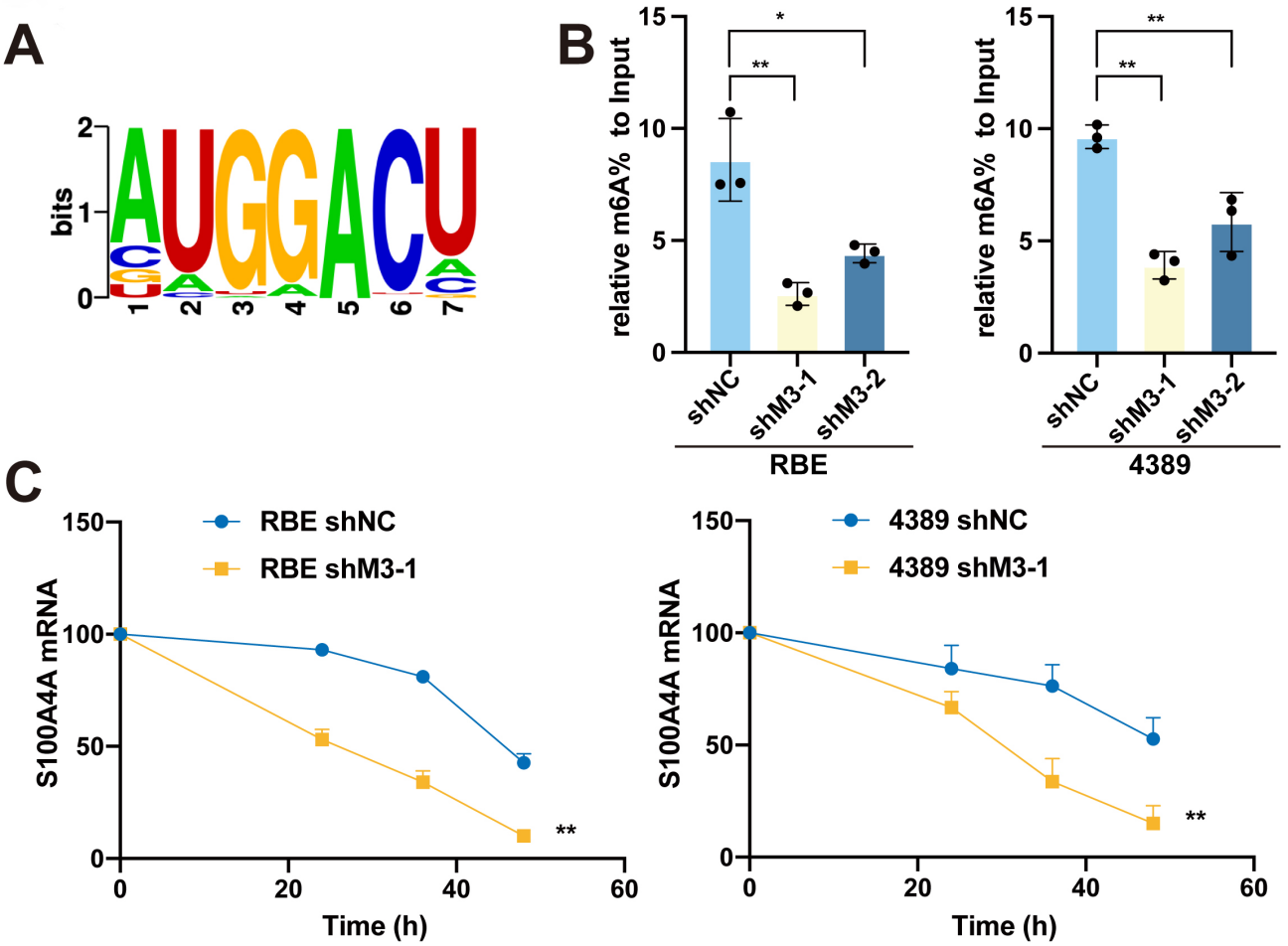

Fig. 6. METTL3 regulates the stability of *S100A4* mRNA. (A) Predicted S100A4 m6A modification sites in the RMbase database. (B) Relative quantification of *S100A4* mRNA m6A modification levels in RBE and 4389 cells from diverse groups (shNC, shM3-1 and shM3-2, n = 3). (C) The half-life ($t_{1/2}$) of *S100A4* mRNA in ICC cells from distinct groups (shNC and shM3-1, n = 3). *$p < 0.05$; **$p < 0.01$.

QC *et al.* [13] and Gao J *et al.* [14], further consolidating the oncogene role of METLL3 in ICC and elucidating its influence on ICC proliferation, migration, and invasion.

Although the vital role of METTL3 and its regulated downstream targets in ICC has been reported in the literature, such as IFIT2 [13], NFAT5 [14], and HLF [15], IFIT2 is a straightforward target of the IFN-Is response and plays a crucial role in innate immune response [31]. NFAT5 acts as a tonic regulatory transcription factor (Ton/EBP) that controls gene expressions related to osmolality [32], resulting in elevated glycolytic activity in ICC cells, upregulating GLUT1 and PGK1, thereby promoting ICC development. HLF, a transcription factor, can be mediated by METTL3 and m6A modification in ICC cells. Through high-throughput sequencing, we explored the differentially expressed genes after interfering with METTL3 and identified S100A4 as an EMT-related molecule. Several studies have demonstrated that *S100A4* enhances the proliferation and metastasis of various cancers, including cholangiocarcinoma [33,34]. Furthermore, S100A4 has been associated with low postoperative survival in ICC patients [35] and may be a valuable marker for predicting ICC progression, metastasis, and prognosis [9]. We found that changes in the proliferation, migration, and invasion abilities of ICC cells affected by METTL3 were partially restored after the overexpression of S100A4. Additionally, combined with the predicted m6A modification site of S100A4 in the RMBase database, we confirmed that S100A4 was indeed regulated by METTL3-mediated m6A modification.

Furthermore, interference with METTL3 significantly reduced the mRNA half-life of S100A4, indicating that METTL3 can affect the expression of *S100A4* by mediating the m6A in *S100A4* mRNA, thereby impacting its expression levels. Thus, we confirmed that the promotive effect of METTL3 on ICC is mediated through S100A4 regulation, revealing a novel regulatory mechanism of ICC different from previous studies. However, our study has some limitations. For example, we could not construct m6A-modifying mutants of S100A4 or further clarify their role in ICC, necessitating in-depth investigations.

In conclusion, our findings demonstrate that METTL3 plays a pro-cancerous role in ICC, and METTL3 can promote the expression of *S100A4* by regulating the m6A methylation modification level of its downstream molecule *S100A4* mRNA, prolonging its mRNA half-life, thus promoting the progression of ICC.

Conclusions

In summary, METTL3 promotes ICC progression and metastasis by mediating the mRNA degradation of its downstream molecule, S100A4, through m6A methylation.

Availability of Data and Materials

Data are available from the corresponding author on reasonable request.

Author Contributions

Conceptualization, JS and ZM; methodology, JS and CZ; software, JS; validation, JS, YZ and ZM; formal analysis, JS, CH; investigation, JS and CZ; resources, JS and ZM; data curation, JS and ZM; writing—original draft preparation, JS; writing—review and editing, JS; visualization, JS; supervision, ZM; project administration, ZM. All authors have read and agreed to the published version of the manuscript. All authors contributed to important editorial changes in the manuscript. All authors have participated sufficiently in the work and agreed to be accountable for all aspects of the work.

Ethics Approval and Consent to Participate

The study was conducted following the Declaration of Helsinki and approved by the Ethics Committee of Fudan University Shanghai Cancer Center, China (FUSCC-IACUC-S2022-0622). All the study participants provided written informed consent. All animals were lawfully acquired and their retention and use were in every case in compliance with federal, state and local laws and regulations, and in accordance with the Institutional Animal Care and Use Committee of SHCO (IACUC) Guide for Care and Use of Laboratory Animals (SHCO-20200042).

Acknowledgment

Not applicable.

Funding

This research received no external funding.

Conflict of Interest

The authors declare no conflict of interest.

Supplementary Material

Supplementary material associated with this article can be found, in the online version, at https://doi.org/10.23812/j.biol.regul.homeost.agents.20243809.466.

References

[1] Banales JM, Marin JJG, Lamarca A, Rodrigues PM, Khan SA, Roberts LR, *et al*. Cholangiocarcinoma 2020: the next horizon in mechanisms and management. Nature Reviews. Gastroenterology & Hepatology. 2020; 17: 557–588.

[2] Ilyas SI, Khan SA, Hallemeier CL, Kelley RK, Gores GJ. Cholangiocarcinoma - evolving concepts and therapeutic strategies. Nature Reviews. Clinical Oncology. 2018; 15: 95–111.

[3] Bridgewater J, Galle PR, Khan SA, Llovet JM, Park JW, Patel T, *et al*. Guidelines for the diagnosis and management of intrahepatic cholangiocarcinoma. Journal of Hepatology. 2014; 60: 1268–1289.

[4] Poultsides GA, Zhu AX, Choti MA, Pawlik TM. Intrahepatic cholangiocarcinoma. The Surgical Clinics of North America. 2010; 90: 817–837.

[5] Spencer K, Pappas L, Baiev I, Maurer J, Bocobo AG, Zhang K, *et al*. Molecular profiling and treatment pattern differences between intrahepatic and extrahepatic cholangiocarcinoma. Journal of the National Cancer Institute. 2023; 115: 870–880.

[6] Thiery JP, Acloque H, Huang RYJ, Nieto MA. Epithelial-mesenchymal transitions in development and disease. Cell. 2009; 139: 871–890.

[7] Kalluri R, Weinberg RA. The basics of epithelial-mesenchymal transition. The Journal of Clinical Investigation. 2009; 119: 1420–1428.

[8] Zeisberg M, Neilson EG. Biomarkers for epithelial-mesenchymal transitions. The Journal of Clinical Investigation. 2009; 119: 1429–1437.

[9] Tian X, Wang Q, Li Y, Hu J, Wu L, Ding Q, *et al*. The expression of S100A4 protein in human intrahepatic cholangiocarcinoma: clinicopathologic significance and prognostic value. Pathology Oncology Research: POR. 2015; 21: 195–201.

[10] Cai X, Wang X, Cao C, Gao Y, Zhang S, Yang Z, *et al*. HBXIP-elevated methyltransferase METTL3 promotes the progression of breast cancer via inhibiting tumor suppressor let-7g. Cancer Letters. 2018; 415: 11–19.

[11] Vu LP, Pickering BF, Cheng Y, Zaccara S, Nguyen D, Minuesa G, *et al*. The N^6-methyladenosine (m^6A)-forming enzyme METTL3 controls myeloid differentiation of normal hematopoietic and leukemia cells. Nature Medicine. 2017; 23: 1369–1376.

[12] Chen M, Wei L, Law CT, Tsang FHC, Shen J, Cheng CLH, *et al*. RNA N6-methyladenosine methyltransferase-like 3 promotes liver cancer progression through YTHDF2-dependent posttranscriptional silencing of SOCS2. Hepatology (Baltimore, Md.). 2018; 67: 2254–2270.

[13] Xu QC, Tien YC, Shi YH, Chen S, Zhu YQ, Huang XT, *et al*. METTL3 promotes intrahepatic cholangiocarcinoma progression by regulating IFIT2 expression in an m^6A-YTHDF2-dependent manner. Oncogene. 2022; 41: 1622–1633.

[14] Gao J, Fang Y, Chen J, Tang Z, Tian M, Jiang X, *et al*. Methyltransferase like 3 inhibition limits intrahepatic cholangiocarcinoma metabolic reprogramming and potentiates the efficacy of chemotherapy. Oncogene. 2023; 42: 2507–2520.

[15] Xiang D, Gu M, Liu J, Dong W, Yang Z, Wang K, *et al*. m6A RNA methylation-mediated upregulation of HLF promotes intrahepatic cholangiocarcinoma progression by regulating the FZD4/β-catenin signaling pathway. Cancer Letters. 2023; 560: 216144.

Journal of
BIOLOGICAL REGULATORS
and Homeostatic Agents

[16] Rokita M, Stec R, Bodnar L, Charkiewicz R, Korniluk J, Smoter M, *et al*. Overexpression of epidermal growth factor receptor as a prognostic factor in colorectal cancer on the basis of the Allred scoring system. OncoTargets and Therapy. 2013; 6: 967–976.

[17] Cheasley D, Fernandez ML, Köbel M, Kim H, Dawson A, Hoenisch J, *et al*. Molecular characterization of low-grade serous ovarian carcinoma identifies genomic aberrations according to hormone receptor expression. NPJ Precision Oncology. 2022; 6: 47.

[18] Hasebe T, Okada N, Tamura N, Houjoh T, Akashi-Tanaka S, Tsuda H, *et al*. p53 expression in tumor stromal fibroblasts is associated with the outcome of patients with invasive ductal carcinoma of the breast. Cancer Science. 2009; 100: 2101–2108.

[19] Li T, Hu PS, Zuo Z, Lin JF, Li X, Wu QN, *et al*. METTL3 facilitates tumor progression via an m^{6}A-IGF2BP2-dependent mechanism in colorectal carcinoma. Molecular Cancer. 2019; 18: 112.

[20] Xu Y, Song M, Hong Z, Chen W, Zhang Q, Zhou J, *et al*. The N6-methyladenosine METTL3 regulates tumorigenesis and glycolysis by mediating m6A methylation of the tumor suppressor LATS1 in breast cancer. Journal of Experimental & Clinical Cancer Research: CR. 2023; 42: 10.

[21] Chen H, Pan Y, Zhou Q, Liang C, Wong CC, Zhou Y, *et al*. METTL3 Inhibits Antitumor Immunity by Targeting m^{6}A-BHLHE41-CXCL1/CXCR2 Axis to Promote Colorectal Cancer. Gastroenterology. 2022; 163: 891–907.

[22] Wang L, Yang Q, Zhou Q, Fang F, Lei K, Liu Z, *et al*. METTL3-m^{6}A-EGFR-axis drives lenvatinib resistance in hepatocellular carcinoma. Cancer Letters. 2023; 559: 216122.

[23] Wang Q, Chen C, Ding Q, Zhao Y, Wang Z, Chen J, *et al*. METTL3-mediated m^{6}A modification of HDGF mRNA promotes gastric cancer progression and has prognostic significance. Gut. 2020; 69: 1193–1205.

[24] Song H, Song J, Cheng M, Zheng M, Wang T, Tian S, *et al*. METTL3-mediated m^{6}A RNA methylation promotes the anti-tumour immunity of natural killer cells. Nature Communications. 2021; 12: 5522.

[25] Zhu L, Li B, Li R, Hu L, Zhang Y, Zhang Z, *et al*. METTL3 suppresses pancreatic ductal adenocarcinoma progression through activating endogenous dsRNA-induced anti-tumor immunity. Cellular Oncology (Dordrecht). 2023; 46: 1529–1541.

[26] Liu W, Zhang Z, Luo X, Qian K, Huang B, Liang J, *et al*. m^{6}A mediated LINC02038 inhibits colorectal cancer progression via regulation of the FAM172A/PI3K/AKT pathway via competitive binding with miR 552 5p. International Journal of Oncology. 2023; 63: 81.

[27] He T, Xia H, Chen B, Duan Z, Huang C. m6A Writer METTL3-Mediated lncRNA LINC01125 Prevents the Malignancy of Papillary Thyroid Cancer. Critical Reviews in Immunology. 2023; 43: 43–53.

[28] Li X, Tang J, Huang W, Wang F, Li P, Qin C, *et al*. The M6A methyltransferase METTL3: acting as a tumor suppressor in renal cell carcinoma. Oncotarget. 2017; 8: 96103–96116.

[29] Jia R, Chai P, Wang S, Sun B, Xu Y, Yang Y, *et al*. m^{6}A modification suppresses ocular melanoma through modulating HINT2 mRNA translation. Molecular Cancer. 2019; 18: 161.

[30] Deng R, Cheng Y, Ye S, Zhang J, Huang R, Li P, *et al*. m^{6}A methyltransferase METTL3 suppresses colorectal cancer proliferation and migration through p38/ERK pathways. OncoTargets and Therapy. 2019; 12: 4391–4402.

[31] Ivashkiv LB, Donlin LT. Regulation of type I interferon responses. Nature Reviews. Immunology. 2014; 14: 36–49.

[32] Kumar R, DuMond JF, Khan SH, Thompson EB, He Y, Burg MB, *et al*. NFAT5, which protects against hypertonicity, is activated by that stress via structuring of its intrinsically disordered domain. Proceedings of the National Academy of Sciences of the United States of America. 2020; 117: 20292–20297.

[33] Cadamuro M, Spagnuolo G, Sambado L, Indraccolo S, Nardo G, Rosato A, *et al*. Low-Dose Paclitaxel Reduces S100A4 Nuclear Import to Inhibit Invasion and Hematogenous Metastasis of Cholangiocarcinoma. Cancer Research. 2016; 76: 4775–4784.

[34] Fabris L, Cadamuro M, Moserle L, Dziura J, Cong X, Sambado L, *et al*. Nuclear expression of S100A4 calcium-binding protein increases cholangiocarcinoma invasiveness and metastasization. Hepatology (Baltimore, Md.). 2011; 54: 890–899.

[35] Tian X, Cao Z, Ding Q, Li Z, Zhang C. Prognostic value of multiple epithelial mesenchymal transition-associated proteins in intrahepatic cholangiocarcinoma. Oncology Letters. 2019; 18: 2059–2065.